Materials Science in Semiconductor Processing 56 (2016) 29–36

Contents lists available at ScienceDirect

Materials Science in Semiconductor Processing

journal homepage: www.elsevier.com/locate/mssp

Enhancing current density of perovskite solar cells using TiO_2-ZrO_2 composite scaffold layer

M. Che, L. Zhu, Y.L. Zhao *, D.S. Yao, X.Q. Gu, J. Song, Y.H. Qiang

School of Materials Science and Engineering, China University of Mining and Technology, Xuzhou 221116, China

ARTICLE INFO

Article history:
Received 12 January 2016
Received in revised form
24 June 2016
Accepted 9 July 2016

Keywords:
TiO_2-ZrO_2 composite
Photoanode
Mesoporous structure
Perovskite solar cells

ABSTRACT

A novel scaffold layer composed of TiO_2-ZrO_2 composite was fabricated for perovskite solar cell. Compared with pure TiO_2 nanoparticles (NPs), the relatively larger ZrO_2 NPs could increase film roughness and enhance light-scattering effect in TiO_2-ZrO_2 composite films. The device exhibited outstanding power conversion efficiency (PCE) of 11.41%. The morphology and aggregation of particles, three-dimensional roughness, as well as the ingredient and micro-structure of FTO/compact TiO_2/TiO_2-ZrO_2 was investigated by scanning electron microscopy (SEM), transmission electron microscopy (TEM), atomic force microscope (AFM), energy dispersive spectrometer (EDS), and X-ray diffraction (XRD), respectively. Moreover, the optical property of TiO_2-ZrO_2 films for visible light was characterized by UV–visible absorption spectroscopy (UV–vis), and its influence on quantum yield of the device was further demonstrated by incident photon-to-electron conversion efficiency (IPCE). Owing to the inert oxide, the short-circuit current density of perovskite solar cell using TiO_2-ZrO_2 composition as scaffold layer increased by 21% compared to the one employing pure TiO_2 mesoporous film.

1. Introduction

Recently, organic-inorganic hybrid perovskite solar cells (PSCs) have become a research frontier of photovoltaic technology, because of their low cost and excellent performance. In an article published in 2009, Miyasaka synthesized an organometal halide ($CH_3NH_3PbI_3$) as visible-light sensitizer for dye-sensitized solar cells (DSSCs) and achieved a power conversion efficiency (PCE) of 3.9% [1]. Up to now, intramolecular exchange was applied to fabricate perovskite layers and the PCE of 20.1% was confirmed by Seok and co-workers [2]. Typically, a layered sandwich-type structure is adopted in PSCs, including transparent FTO substrate, electron transport layer, mesoporous layer, perovskite light harvester layer, hole transport layer, as well as metal back electrode [3–5]. It has been proved to be an effective way to enhance carrier transport rate and suppress energy losses by controlling the structure and morphology of the mesoporous layer [6,7].

Owing to the excellent optical property and the suitable bandgap [8], TiO_2 as a traditional electron extraction material is widely applied in PSCs based on mesoporous structure [9,10]. The thickness of mesoporous TiO_2 layer was controlled, leading to the best PCE exceeding 9% [11,12]. Subsequently, meso-superstructured solar cells invented by Snaith and Miyasaka, the n-type scaffold oxides can be replaced by inert mesoporous materials (such as Al_2O_3), remarkably rose the open-circuit photovoltages to as high as 1.1 V and obtained a PCE approaching 11% [13]. Ever since then, a variety of scaffold layers have developed with insulating materials including Al_2O_3 and ZrO_2 [14,15].

According to the advantages of these new-type scaffold layer, we proposed to add a small amount of ZrO_2 NPs into TiO_2 paste to fabricate a composite mesoporous layer for PSCs. We found that the film roughness and light-scattering effect improvement in scaffold layer is favorable for short-circuit current density enhancement for perovskite solar cells. Therefore, perovskite solar cell based on the optimal ZrO_2-TiO_2 composite scaffold layer could achieve a conversion efficiency of 11.41% which is much higher than the one with conventional TiO_2 scaffold layer (9.86%).

2. Materials and methods

2.1. Preparation of TiO_2-ZrO_2 paste

The concentrated aqueous ammonia was dropwise added in a volume of 100 mL solution of zirconium oxychloride (0.1 mol/L) to adjust a pH of 9.5. After centrifuging at 3000 rpm, the prepared solution was washed three times by deionized water to insure that the flocculent precipitate cannot generate when the sample was titrated by $AgNO_3$ (0.1 mol/L). A volume of 10 mL of the sol and an equal volume of distilled water was added Teflon autoclave, which

* Corresponding author.
E-mail address: sdyulong@cumt.edu.cn (Y.L. Zhao).

http://dx.doi.org/10.1016/j.mssp.2016.07.003
1369-8001/

was put in oven at 250 °C for 48 h. After cooling to room temperature, the residual liquid was removed and the ZrO_2 powder was dried at 60 °C. The ZrO_2 powder/absolute ethyl alcohol ratio is 1:12, 1:30 and 1:60 by weight, respectively. The dispersed solution A was achieved via violent stirring for 1 h. Dyesol 18 NRT was diluted in absolute ethanol in a proportion of 1:3.5 by weight under vigorous stirring for 1 h which was denoted as solution B. Then, polyethylene glycol-400 (approximately 2% in weight) and dispersion solution A was dropwise added in solution B under stirring. In the end, TiO_2-ZrO_2 mixture with different concentration was formed by stirring the mixed solution overnight.

2.2. Device fabrication

F-doped SnO_2 (FTO, 2.2 mm thick, < 15 Ω/sq, Opvtech) glass substrates were etched with the turbid solution of Zn powder and concentrated hydrochloric acid, and cleaned under ultrasonication. Subsequently, the ultrathin blocking compact layer of TiO_2 was fabricated by spin-coating the TiO_2 sol-gel at 4500 rpm for 30 s, and then annealed at 450 °C for 60 min in a furnace under ambient air. For the preparation of scaffold layer, the TiO_2-ZrO_2 composite paste was spin-coated on the compact TiO_2 layer at 5000 rpm for 30 s, which was then dried at 130 °C for 10 min and sintered at 500 °C for 15 min in air. The PbI_2/DMF solution (462 mg/mL) was infiltrated into the mesoporous film by spin-coating at 5000 rpm for 30 s and annealed at 70 °C for 30 min in a glove box. The film was cooled to room temperature and immersed into a solution of methylammonium iodide (CH_3NH_3I, MAI, 10 mg/mL) dissolved in 2-propanol for 150 s. The white powder of MAI was synthesized according to early reports [16,17]. After that, the film was put on a hotplate at 70 °C for 30 min 50 μL hole transport materials (HTMs) were spin-coated on the perovskite layer at 3000 rpm for 30 s. The HTM solution was prepared by dissolving 72.3 mg (2,2′,7,7′-tetrakis(N,N-di-*p*-meth-oxyphenylamine)-9,9-spirobi-fluorene) (spiro-Me-OTAD), 28.8 μL 4-tert-butylpyridine (TBP), 17.5 μL of bis(trifluoromethylsulphonyl)-imide (LiTFSI) in acetonitrile (520 mg/mL) in 1 mL chlorobenzene. Finally, the 55 nm of Ag as counter electrode was evaporated using thermal evaporator on the HTMs-coated film.

2.3. Characterization

The morphology of mesoscopic thin films with and without $CH_3NH_3PbI_3$ deposition were characterized by field-emission scanning electron microscopy (FESEM, 1530VP, LEO). The elemental analysis of TiO_2-ZrO_2 composite films was carried out by SEM equipped with energy-dispersive X-ray spectroscopy (EDX, 1530VP, LEO). The ZrO_2 and ZrO_2-TiO_2 composite particles were characterized by transmission electron microscopy (TEM, Tecnai G2 F20). The structure of TiO_2, TiO_2-ZrO_2, PbI_2 and $CH_3NH_3PbI_3$ were measured by X-ray diffraction (XRD, Bruker D8 Advance, Germany). The optical properties of different films were recorded by a spectrophotometer (UV–vis, Cary-300 Varian). The three-dimensional roughness of scaffold layer was measured with the atomic force microscope (AFM, CSPM5500). The current density-voltage (*J-V*) curves of perovskite solar cells were carried out by an electrochemical workstation (Keithley, 2420 Source Meter), and the devices were illuminated by a solar simulator (Oriel Sol 3A, Newport) under 100 mW cm^{-2} irradiation. The aperture area of devices was controlled at 0.1 cm^2 by a metal mask during the measurement. The incident photon-to-electron conversion efficiency (IPCE) spectrum for perovskite solar cells were measured by a Newport IPCE system (Newport, USA).

3. Results and discussion

As shown in Fig. 1(a), the samples of different ZrO_2-TiO_2 composites deposited on glass are characterized by XRD in order to avoiding the interference of FTO substrates. Clearly, the peaks appeared at 25.28°, 48.05° and 37.8° in each spectrum are in consistent with standard TiO_2 anatase structure (JCPDS#21-1272). For 1.25% ZrO_2-TiO_2 film, no clear distinction could be observed as the small amount of ZrO_2. However, an intense diffraction peak appears at 28.17°when the amounts of ZrO_2 NPs is 2.5% and 5%, manifesting the successful incorporation of ZrO_2 NPs into TiO_2 paste. Fig. 1(b) displays distinct patterns of PbI_2 and $CH_3NH_3PbI_3$ films. A strong diffraction peak of (001) at 12.6° occurs in PbI_2 film, which is in consistent with the previous report [3]. The tetragonal $CH_3NH_3PbI_3$ is confirmed by diffraction peaks at 14.13°, 28.43° and 38.03°, reflecting the (110), (220), and (330) lattice planes, respectively.

Fig. 2(a) shows a conventional mesoporous structure of TiO_2, which provides supporting framework for $CH_3NH_3PbI_3$. When the ZrO_2 NPs are doped into TiO_2 paste, bright particles emerge. Besides, the density of these bright particles rise with the increase of ZrO_2 added in the paste (Fig. 2(b)–(d)). The serious agglomeration of bright particles appear when the concentration of ZrO_2 is 5%. The sample of 2.5% ZrO_2-TiO_2 shows a relatively homogeneous coexistent form compared with other concentration. The morphology of perovskite is presented in Fig. 2(e) and (f). The $CH_3NH_3PbI_3$ cuboids are closely distributed on the scaffold layer

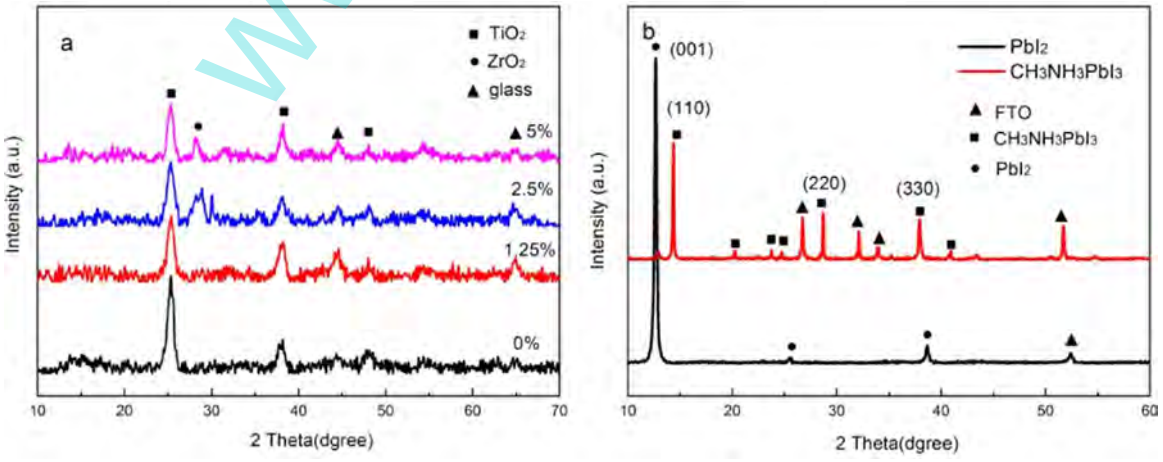

Fig. 1. XRD patterns of (a) ZrO_2-TiO_2 composite films with varied ZrO_2 based on glass substrate, (b) PbI_2 and $CH_3NH_3PbI_3$ covered on 2.5% ZrO_2-TiO_2 scaffold layer based on FTO glass substrate.

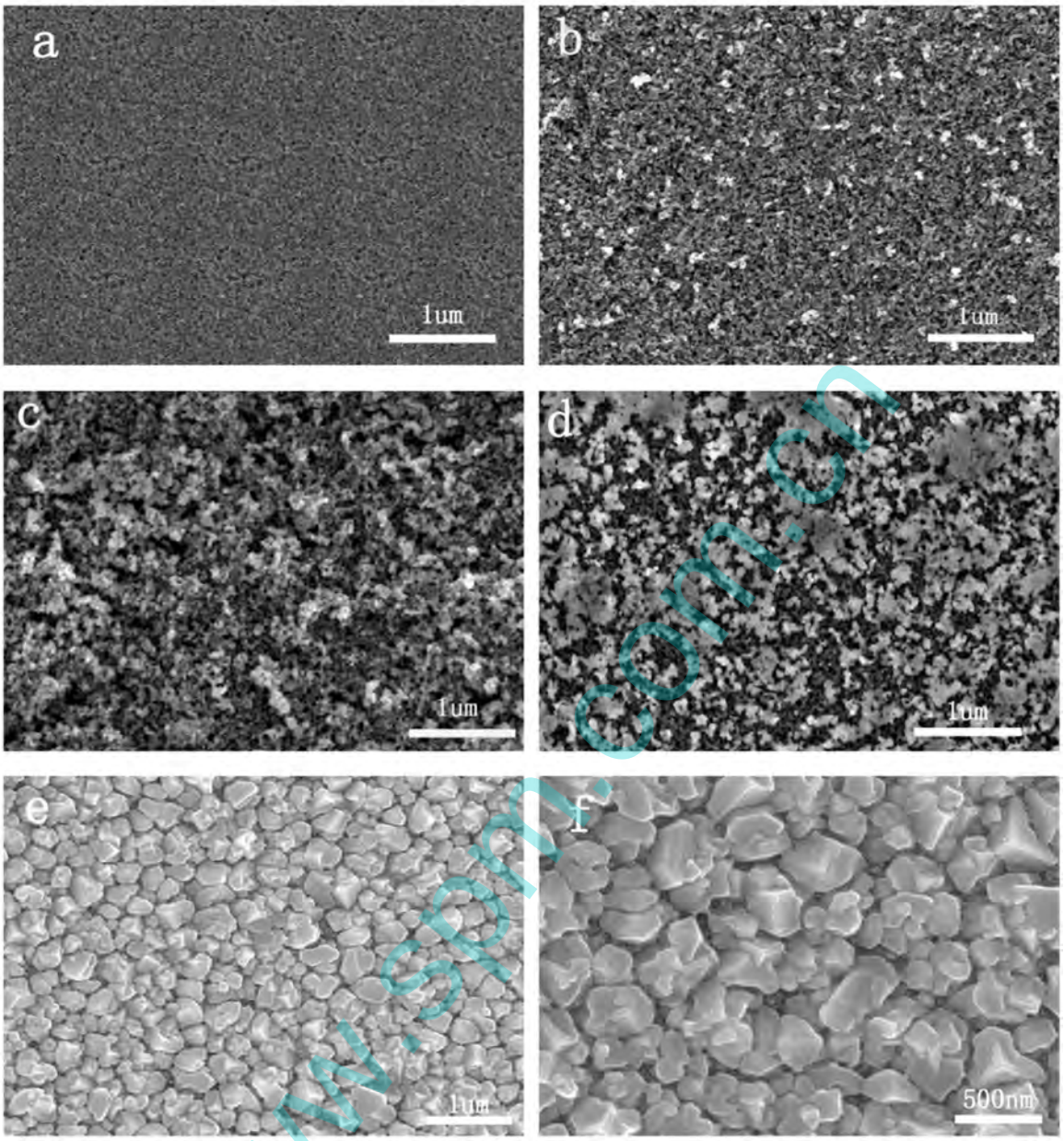

Fig. 2. SEM images of ZrO_2-TiO_2 scaffold layers with different amount of ZrO_2 (a) 0 wt%, (b) 1.25 wt%, (c) 2.5 wt%, (d) 5 wt%. SEM images of $CH_3NH_3PbI_3$ films covered on 2.5% ZrO_2-TiO_2 scaffold layer, (e) low resolution and (f) high resolution.

and this is similar to the morphology of perovskite films in previous report [3]. To demonstrate composition of the bright particles in above SEM images, EDX is carried out for the 2.5% TiO_2-ZrO_2 composite film. As shown in Fig. 3(a) and (b), Zr atom is detected in the selected area. Furthermore, elemental mapping in the selected area exhibits that brightness of Zr is in accordance with distribution of the bright particles in the SEM images while Ti and O mapping are compact and uniform (Fig. 3(c)–(f)). Therefore, we believe that the bright particles should be ZrO_2.

TEM images of ZrO_2 and ZrO_2-TiO_2 composite particles are shown in Fig. 4. The morphologies of ZrO_2 powders are quite similar to each other, and their diameters range from 40 to 100 nm (Fig. 4a). In comparison with ZrO_2, TiO_2 particles have smaller particle sizes (around 20 nm), as shown in Fig. 4(b). From EDX spectra in Fig. 4(c), the peaks of Ti, Zr and O indicate that the powders are ZrO_2-TiO_2 composite.

Atomic force microscope (AFM) is applied to further dissect the morphology, structure and uniformity of these novel scaffold layers, as shown in Fig. 5. The surface roughness is measured to be 42.2 nm for 5%, 26.6 nm for 2.5%, 16.1 nm for 1.25% and 23.4 nm for pure TiO_2, respectively (Fig. 5(b1)–(b4)). The diagonal line roughness is also characterized to be 36 nm for 5%, 25.3 nm for 2.5%, 15.8 nm for 1.25% and 21.9 nm for pure TiO_2 (Fig. 5(c1)–(c4)). The smoothest film is formed by spin-coating 1.25% ZrO_2-TiO_2 paste and film roughness turn higher as more ZrO_2 particles are added in scaffold layer. It should be noted that the film formed by spin-coating 1.25% ZrO_2-TiO_2 paste showed lower roughness than that for pristine TiO_2. The result may be caused by the fact that the void formed pristine TiO_2 film might be filled by a negligible quantity of ZrO_2 particle. The crucial role of mesoscopic film in PSCs is to provide support frame for $CH_3NH_3PbI_3$ [13]. Film roughness is a key indicator to evaluate $CH_3NH_3PbI_3$ loading capacity of scaffold layer. In fact, rough surface could provide more passages for PbI_2 infiltration compared to a smooth one. In other words, rough surface film may hold more $CH_3NH_3PbI_3$ particles in photoanode. The influence of scaffold film roughness on

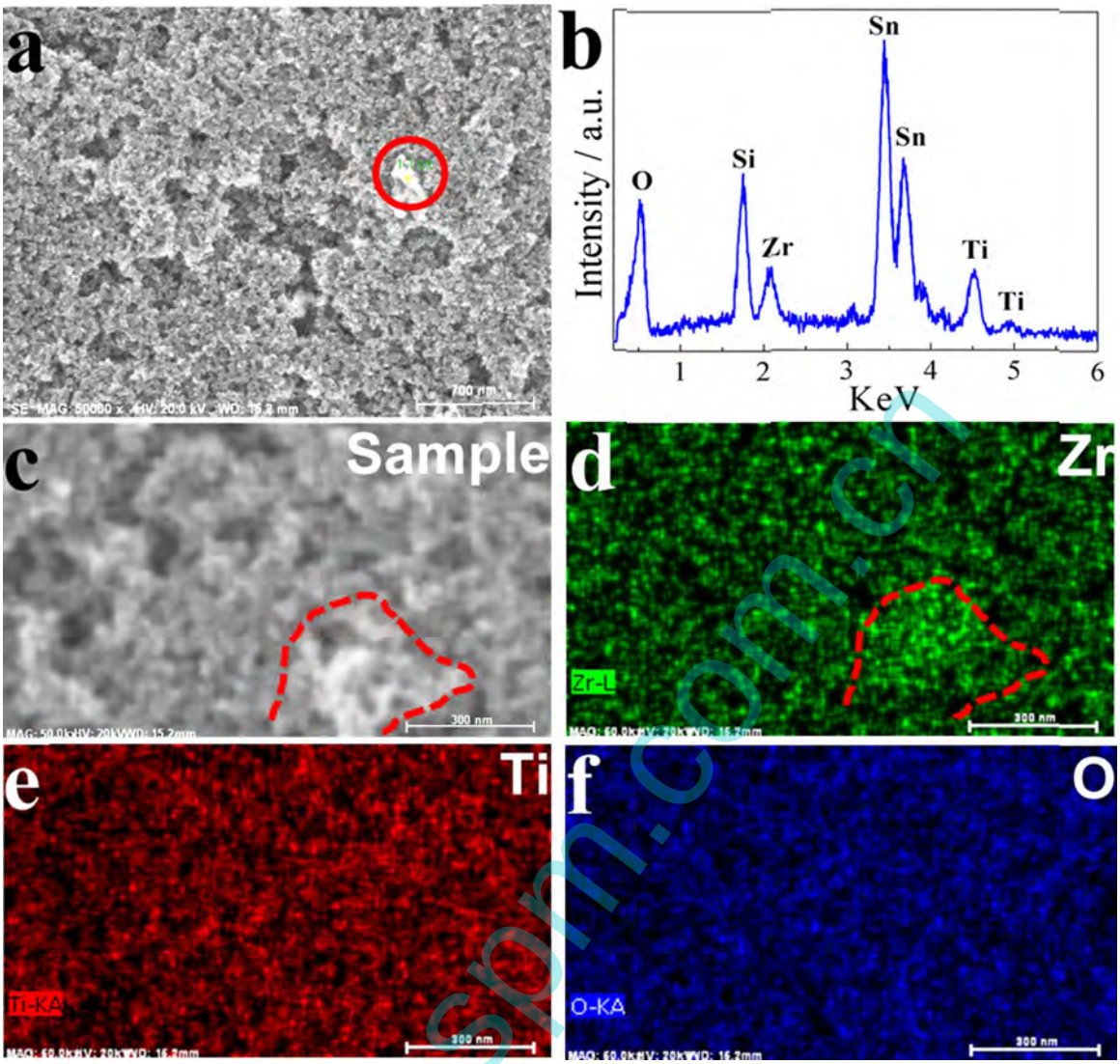

Fig. 3. (a) SEM image and (b) corresponding EDX spectra of selected area, (c)–(f) SEM image and elemental mapping (Zr, Ti, O) of the 2.5% ZrO_2-TiO_2 film.

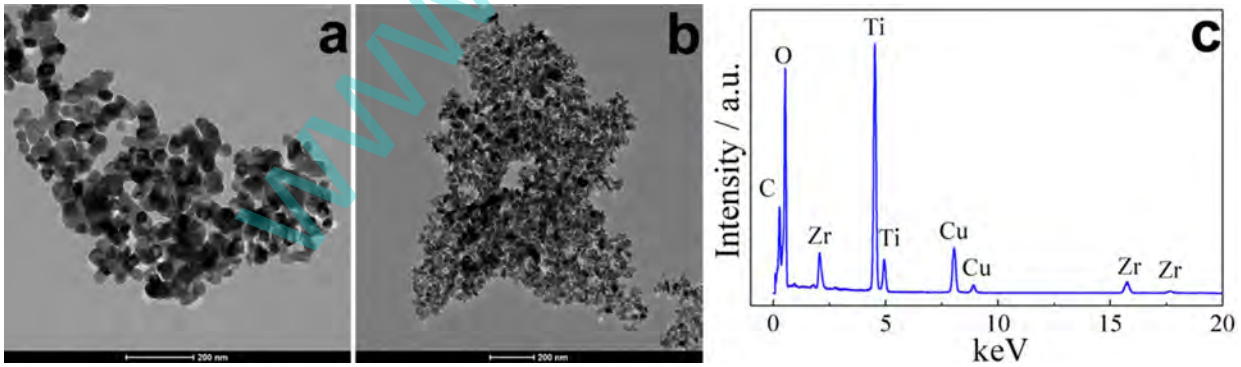

Fig. 4. TEM images of (a) ZrO_2 NPs and (b) 2.5% ZrO_2-TiO_2 composite. (c) EDX spectra of the area in (b).

photovoltaic performance of corresponding PSCs will be discussed later.

The optical property of mesoscopic films is closely related to the composition of TiO_2-ZrO_2 composite. As seen in Fig. 6(a), the addition of ZrO_2 NPs slightly decrease the visible light absorption intensity of scaffold films, compared with pure TiO_2 mesoscopic film. Meanwhile, the light reflection ability of scaffold films increase a little as the addition of ZrO_2. Therefore, we speculate that ZrO_2 particle in scaffold layer might enhance light scatter although the grain size of ZrO_2 is smaller than 100 nm. We also measured UV–vis absorption spectra of perovskite film, as shown in Fig. 6(c). Apparently, a remarkable enhancement of absorption intensity appears with introducing ZrO_2 NPs in scaffold film. This light absorption enhancement could be ascribed to film roughness increase and light scatter improvement as ZrO_2 addition.

The *J-V* curves of PSCs with different photoanodes are displayed

in Fig. 7, and the parameters (short-current density (J_{sc}), open-circuit voltage (V_{oc}), fill factor (FF), and PCE) are recorded in Table 1. The PSC using TiO_2 as scaffold layer presents a PCE of 9.86%. When 1.25% ZrO_2 is added in TiO_2, the corresponding PSC shows an approximate performance with PSC using pure TiO_2. As ZrO_2 content increases to 2.5%, the PSC exhibits the best photovoltaic performance with J_{sc} of 17.00 mA/cm^2, V_{oc} of 0.97 V, FF of 68.89%, and PCE of 11.41%. The most remarkable change of all the parameters is J_{sc}. As demonstrated in Fig. 5, scaffold film with 2.5% ZrO_2 has a higher roughness than the pristine TiO_2 film while high roughness is usually benefit for perovskite loading. Moreover, the light-scattering effect is enhanced by introducing ZrO_2 NPs. All the advantages make PSC using ZrO_2-TiO_2 scaffold with 2.5% ZrO_2 achieve the highest J_{sc}. However, as ZrO_2 content increases further

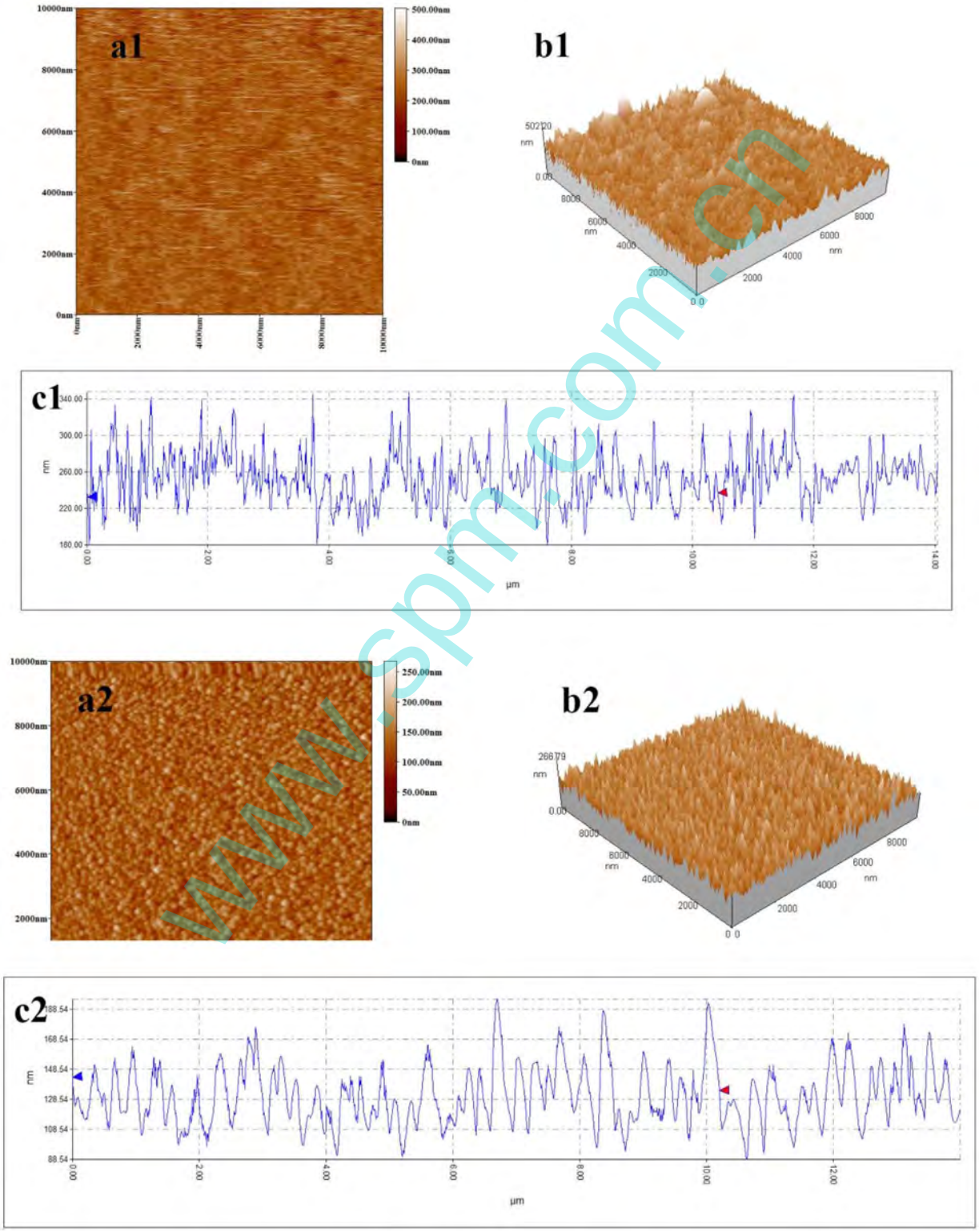

Fig. 5. AFM images of various scaffold layer. (a1–a4) The surface morphologies, (b1–b4) 3D images, (c1–c4) roughness of ZrO_2-TiO_2 in the percentage at 0%, 1.25%, 2.5% and 5%, respectively.

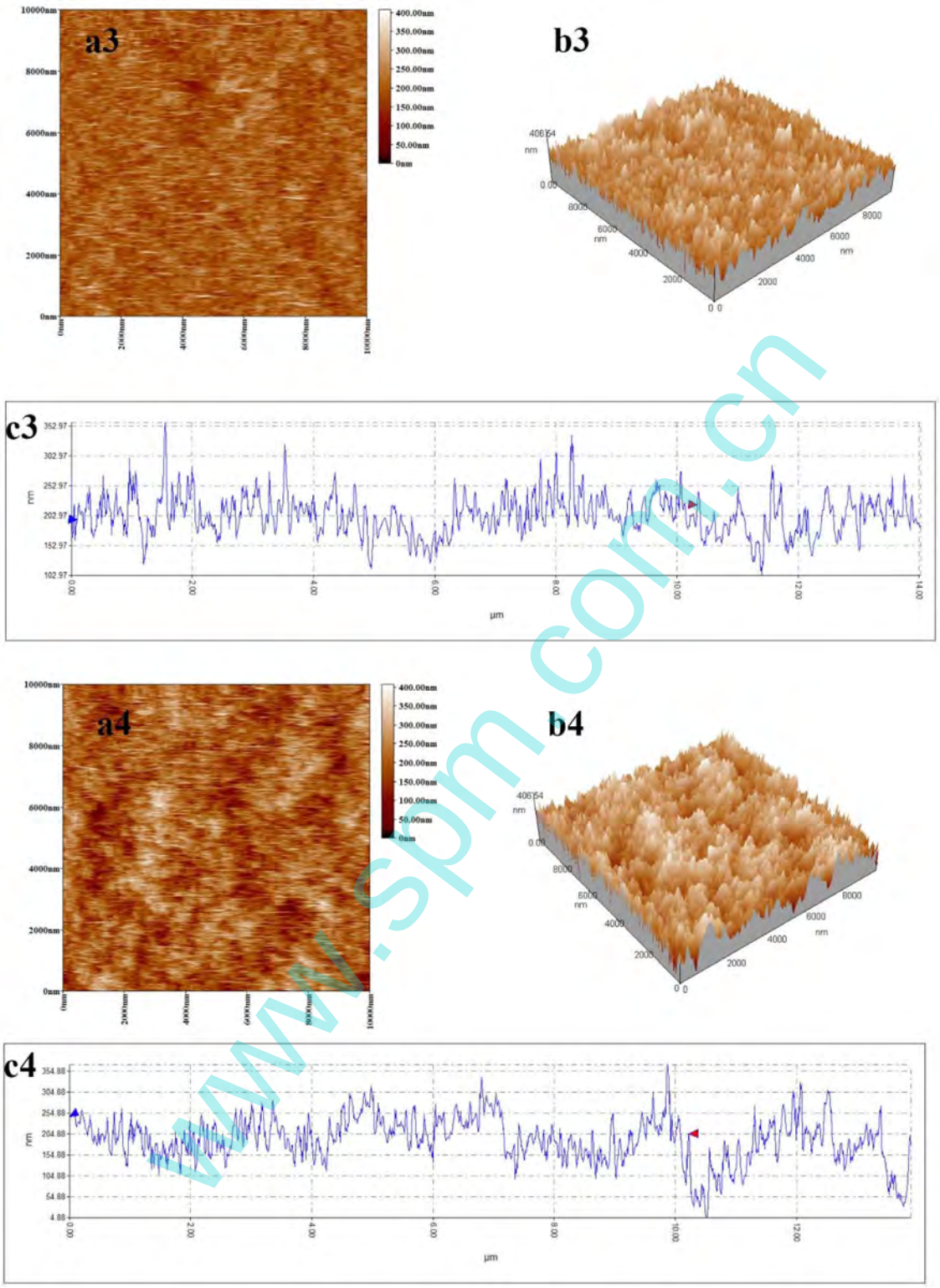

Fig. 5. (*continued*)

to 5%, photovoltaic performance of corresponding PSC decrease sharply. Although light-scattering effect of this scaffold film is the highest, large amount of inert ZrO_2 aggregated in scaffold film is harmful for electron transport from perovskite to compact layer which could decrease V_{oc} of perovskite solar cells. In order to explain V_{oc} decrease with a rise in concentration of ZrO_2, we investigate the interfacial charge kinetics by photoluminescence (PL) measurements. Fig. 8 shows the steady-state PL spectra of perovskite films excited at 450 nm. The PL quenches appears at around 770 nm, which is in consistent with previous report [18]. Moreover, the luminescence is enhanced with the increase of ZrO_2 NPs, indicating that the charge recombination become serious in perovskite film.

The incident photon-to-current conversion efficiency (IPCE) spectra are also sketched in Fig. 9. The change of external quantum efficiency (EQE) is consistent with short-current density of PSCs

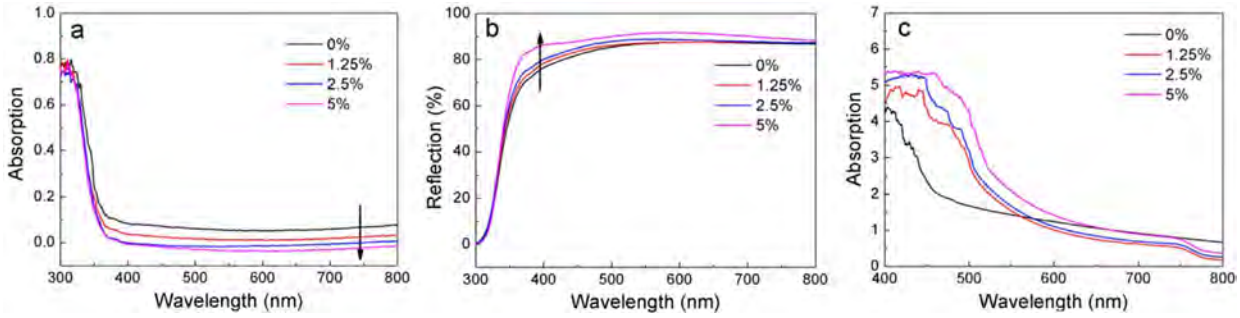

Fig. 6. (a) UV–vis absorption spectra and (b) UV–vis reflection spectra of TiO_2 and ZrO_2-TiO_2 composite films based on glass substrate. (c) UV–vis absorption spectra of $CH_3NH_3PbI_3$ films using TiO_2 and different ZrO_2-TiO_2 scaffold.

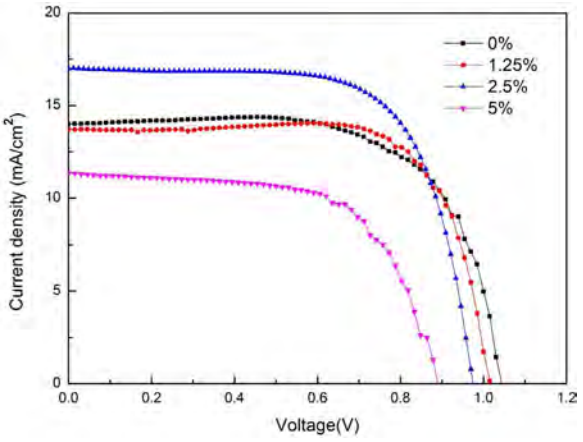

Fig. 7. The current density-voltage (*J-V*) curves of PSCs based on different scaffold layers. All the devices were measured under illumination of 100 mW cm^{-2} and active area of 0.1 cm^2.

Table 1
The best photovoltaic parameters of PSCs with different ZrO_2-TiO_2 scaffold layers.

Samples (%)	J_{sc} (mA/cm^2)	V_{oc} (v)	FF (%)	PCE (%)
0	13.99	1.04	67.57	9.86
1.25	13.70	1.01	73.38	10.19
2.5	17.00	0.97	68.89	11.41
5	11.11	0.88	63.19	6.21

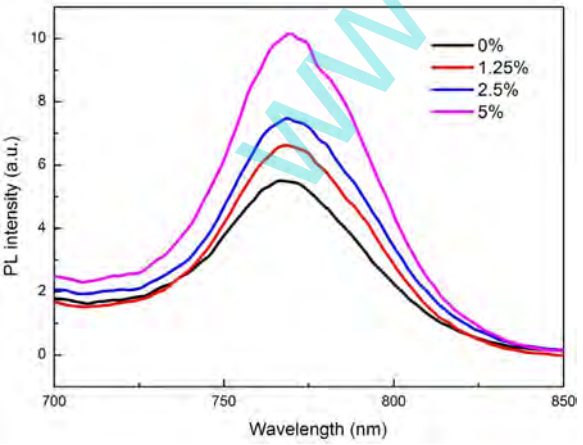

Fig. 8. The PL spectra of $CH_3NH_3PbI_3$ films based on varied scaffold layer.

with different scaffold layers. The optimal EQE value is as high as 87% around 500 nm for PSC using 2.5% ZrO_2-TiO_2. Additionally, we recorded histograms to analyze the floating range of PCE of PSCs

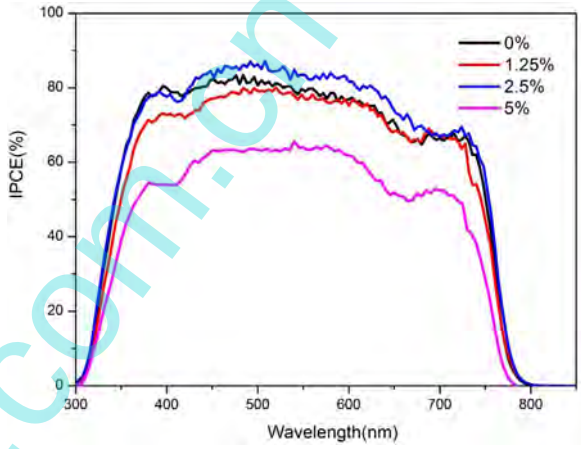

Fig. 9. The IPCE spectra for PSCs based on different photoanodes.

using different scaffold layers, as shown in Fig. 10. We fabricated thirty-five devices for each condition with different ZrO_2 content. As we can see, all of the four histograms follow a Gaussian distribution. Specially, the statistical data of PCE in Fig. 8(c) presents a more narrow range from 9% to 12%. The average PCE is also calculated to be 8.76% for pure TiO_2, 9.62% for 1.25%, 10.7% for 2.5% and 4.82% for 5%. Apparently, the tendency of average PCE exposed by histograms is agree with *J-V* curves.

In fact, electron transporting process in this mesoporous layer is different from that in traditional TiO_2 layer. ZrO_2 has a larger band-gap and their conduction band edge is higher than that of $CH_3NH_3PbI_3$. Therefore, the excited electrons in perovskite active layer could not inject into ZrO_2. As shown in Scheme 1, on the one hand, owing to the inert property of ZrO_2 NPs, the recombination of electrons and holes is enhanced and the V_{oc} of the PSCs decrease. One the other hand, ZrO_2 distributed in scaffold TiO_2 layer could change the direction of light and further enhance the availability of light by light-scattering effect of ZrO_2 NPs which is benefit for current density enhancement in PSCs. The balance between above two factors achieve when ZrO_2/TiO_2 is 2.5% in weight, which exhibit the highest performance as the scaffold layer for perovskite solar cells.

4. Conclusions

In summary, the TiO_2-ZrO_2 composite with different ZrO_2 contents have been synthesized successfully to prepare novel scaffold layer for perovskite solar cells. A high efficiency of 11.41% was achieved for the cell employing 2.5% ZrO_2-TiO_2 composite as mesoscopic thin film. Further study indicated that the power conversion efficiency enhancement was mainly ascribed to the increase of short-current density via light-scattering effect

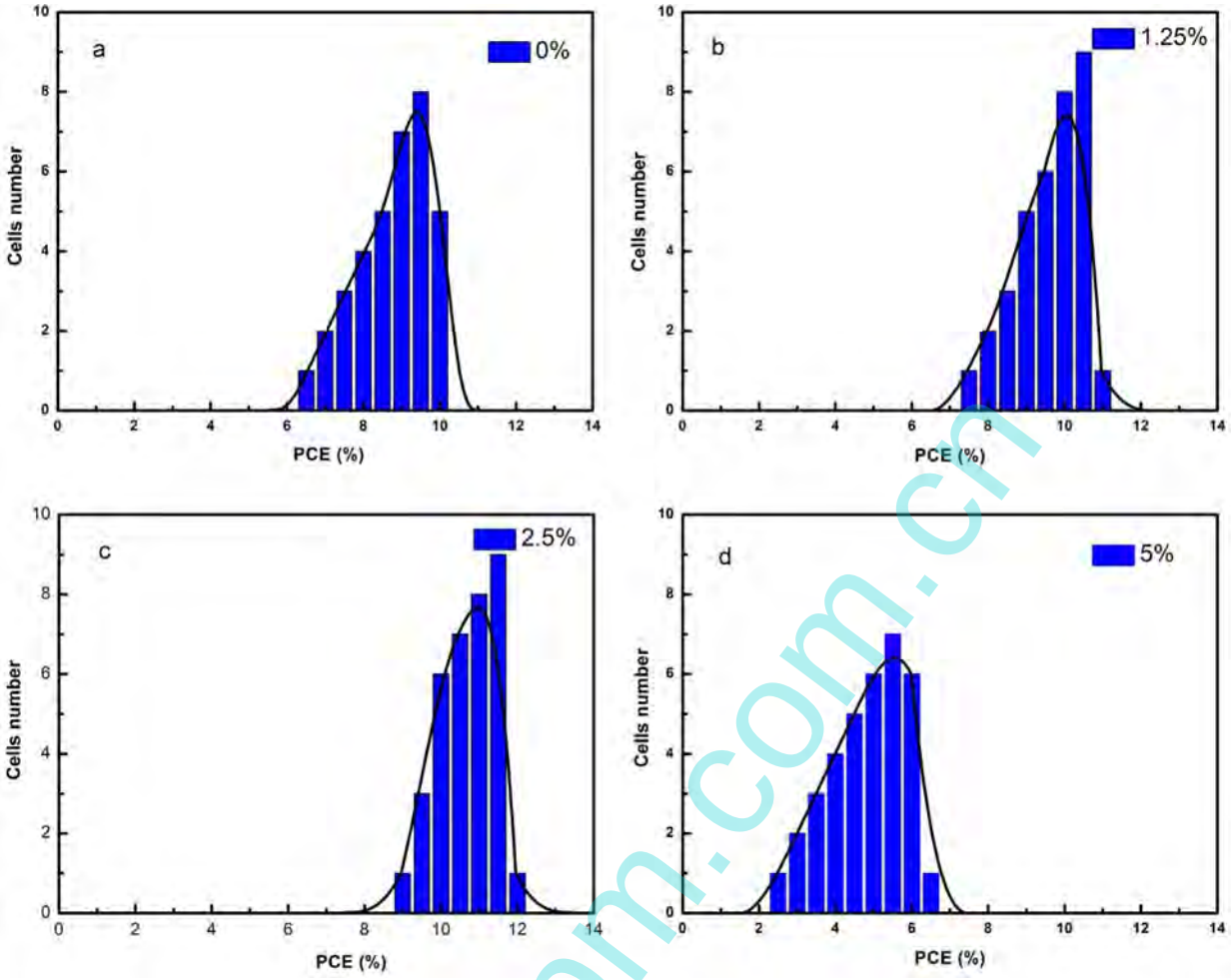

Fig. 10. PCE histograms of PSCs fabricated with various ZrO_2/TiO_2 ratios.

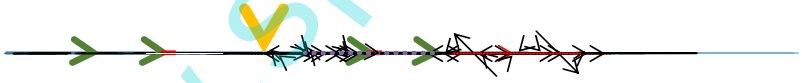

Scheme 1. Schematic description of (a) charge transfer process in photoanode, (b) light-scattering effect enhancement in TiO_2-ZrO_2 composite film.

improvement as the addition of ZrO_2 NPs. In addition, the enhanced film roughness is also beneficial for short-current increase in perovskite solar cells.

Acknowledgments

This work was financially supported by the Fundamental Research Funds for the Central Universities (2015XKMS067).

References

[1] A. Kojima, K. Teshima, Y. Shirai, T. Miyasaka, J. Am. Chem. Soc. 131 (2009) 6050.
[2] W.S. Yang, J.H. Noh, N.J. Jeon, Y.C. Kim, S. Ryu, J. Seo, S.I. Seok, Science 348 (2015) 1234.
[3] J. Burschka, N. Pellet, S. Moon, R. Humphry-Baker, P. Gao, M.K. Nazeeruddin, M. Grätzel, Nature 499 (2013) 316.
[4] J.H. Noh, N.J. Jeon, Y.C. Choi, M.K. Nazeeruddin, M. Grätzel, S. Seok, J. Mater. Chem. A 1 (2013) 11842.
[5] J. Shi, Y. Luo, H. Wei, J. Luo, J. Dong, S. Lv, J. Xiao, Y. Xu, L. Zhu, X. Xu, H. Wu, D. Li, Q. Meng, ACS Appl. Mater. Interfaces 6 (2014) 9711.
[6] T. Leijtens, B. Lauber, G.E. Eperon, S.D. Stranks, H.J. Snaith, J. Phys. Chem. Lett. 5 (2014) 1096.
[7] T. Salim, S.Y. Sun, Y. Abe, A. Krishna, A.C. Grimsdale, Y.M. Lam, J. Mater. Chem. A 3 (2015) 8969.
[8] H.S. Kim, C.R. Lee, J.H. Im, K.B. Lee, T. Moehl, A. Marchioro, S.J. Moon, R. Humphry-Baker, J.H. Yum, J.E. Moser, M. Grätzel, Sci. Rep. 2 (2012) 591.
[9] S.D. Sung, D.P. Ojha, J.S. You, J. Lee, J. Kim, W.I. Lee, Nanoscale 7 (2015) 8898.
[10] P. Qin, A.L. Domanski, A.K. Chandiran, R. Berger, H.-J. Butt, M.I. Dar, T. Moehl, N. Tetreault, P. Gao, S. Ahmad, M.K. Nazeeruddin, M. Grätzel, Nanoscale 6 (2014) 1508.
[11] K. Wang, J. Jeng, P. Shen, Y. Chang, E.W. Diau, C. Tsai, T. Chao, H. Hsu, P. Lin, P. Chen, T. Guo, T. Wen, Sci. Rep. 4 (2014) 4756.
[12] K.C. Wang, P.S. Shen, M.H. Li, S. Chen, M.W. Lin, P. Chen, T.F. Guo, ACS Appl. Mater. Interfaces 6 (2014) 11851.
[13] M.M. Lee, J. Teuscher, T. Miyasaka, T.N. Murakami, H.J. Snaith, Science 338 (2012) 634.
[14] X. Dong, X. Fang, M. Lv, B. Lin, S. Zhang, J. Ding, N. Yuan, J. Mater. Chem. A 3 (2015) 5360.
[15] D.Q. Bi, S.J. Moon, L. Häggman, G. Boschloo, L. Yang, E.M.J. Johansson, M. K. Nazeeruddin, M. Grätzel, A. Hagfeldt, RSC Adv. 3 (2013) 18762.
[16] M. Ramesh, K.M. Boopathi, T.Y. Huang, Y.C. Huang, C. Si. Tsao, C.W. Chu, ACS Appl. Mater. Interfaces 7 (2015) 2359.
[17] Y. Yang, J. Song, Y.L. Zhao, L. Zhu, X.Q. Gu, Y.Q. Gu, M. Che, Y.H. Qiang, J. Alloy. Compd. 684 (2016) 84.
[18] M. Ibrahim Dar, M. Abdi-Jalebi, N. Arora, T. Moehl, M. Grätzel, M. K. Nazeeruddin, Adv. Mater. 27 (2015) 7221.